# Nonstationary pattern-based signal-noise separation using adaptive prediction-error filter[a]

[a]Published in Journal of Geophysics and Engineering, 19, 14-27, (2022)

*Zhisheng Zheng*, Yang Liu*, Cai Liu**

## ABSTRACT

Complex field conditions always create different interferences during seismic data acquisition, and there exist several types of noise in the recorded data, which affect the subsequent data processing and interpretation. To separate an effective signal from the noisy data, we adopted a pattern-based method with a two-step strategy, which involves two adaptive prediction-error filters (APEFs) corresponding to a nonstationary data pattern and noise pattern. By introducing shaping regularization, we first constructed a least-squares problem to estimate the filter coefficients of the APEF. Then, we solved another constrained least-square problem corresponding to the pattern-based signal-noise separation, and different pattern operators are adopted to characterize random noise and ground-roll noise. In comparison with traditional denoising methods, such as FXDECON, curvelet transform and local time-frequency (LTF) decomposition, we examined the ability of the proposed method by removing seismic random noise and ground-roll noise in several examples. Synthetic models and field data demonstrate the validity of the strategy for separating nonstationary signal and noise with different patterns.

## INTRODUCTION

During seismic data acquisition, complex field conditions unavoidably lead to several interferences. For instance, wind motion and electronic noise from geophones cause random noise, propagation of seismic waves on land near the surface leads to ground-roll noise. Meanwhile, it is natural that geologic events and geophysical data exhibit nonstationarity, which is manifested in several intrinsic properties, e.g. spectra and statistical characteristics, and change with time and space. To reduce the influences of noise and improve the quality of useful signal for subsequent data processing and interpretation, the signal-noise separation is always an important procedure, especially in new acquisition techniques such as distributed acoustic sensing.

Many effective methods have been proposed for eliminating seismic random noise besides mean and median filters tailored to images. According to the different properties of target signals, several transform methods can truncate the energy in the

transform domain to suppress random noise, such as radon transform (Claerbout and Johnson, 1971; Trad et al., 2002), curvelet transform (Kumar and Herrmann, 2009) and seislet transform (Fomel and Liu, 2010; Liu et al., 2015). Prediction filters are effective methods for random noise attenuation, which was first introduced by Canales (1984). The prediction process can be achieved in the time-space domain or the frequency-space domain (Wang, 1999). Liu and Li (2018) proposed a fast-streaming prediction filter to attenuate random noise. Recently, the deep-learning method has also been found to cope with the denoising procedure; Yu et al. (2019) developed a deep-learning method for random noise attenuation by using a convolutional neural network.

Ground-roll noise is a strong coherent noise, which will interfere with land seismic surveys. Frequency-based filtering and F-K filtering are the classical methods to handle ground- roll noise problem. Wavelet transform (Miao and Cheadle, 1998; Corso et al., 2003) and curvelet transform (Naghizadeh and Sacchi, 2018) are practical methods for ground-roll removal as well. Time-frequency analysis can separate different components by using a muting filter in the time-frequency domain, Liu and Fomel (2013) applied this method to separate the ground-roll noise from the field data. Using a generator and discriminator, a generative adversarial network (GAN) can be trained to produce a noise-free result, Yuan et al. (2020) developed GAN for ground-roll noise removal.

A pattern-based method is often used for signal-noise separation. Spitz (1999) described a multiple subtraction technology by using a pattern recognition method. Bednar and Neale (1999) made a comparison of a pattern-based multiple suppression method and other approaches. Brown and Clapp (2000) used a pattern-based method with nonstationary prediction-error filter (PEF) for ground-roll removal. Guitton (2006) further implemented such a pattern-based approach to separate multiples in a 3D dataset.

In this paper, we revisit the fundamental theory behind the pattern-based signal-noise separation method (Claerbout, 2010) and extend this with an adaptive prediction-error filter (APEF). The pattern-based method (Brown and Clapp, 2000; Claerbout and Fomel, 2000) estimates operators to characterize data patterns, and then solves the signal-noise separation problem. Similarly, we exploited the pattern-based method but calculated the APEF (Liu et al., 2011) to represent the pattern of nonstationary data and the noise model. Different algorithms were adopted to deal with random noise and ground-roll noise, and we tested the nonstationary characteristics of the proposed method in synthetic models and field data examples. Results of random noise attenuation and ground-roll removal on these examples demonstrated that the pattern-based signal-noise separation with the nonstationary APEF is effective in separating noise from signal.

# THEORY

## Signal and noise separation problem

A simple assumption is that the dataset $\mathbf{d}$ can be considered as the summation of signal $\mathbf{s}$ and noise $\mathbf{n}$:

$$\mathbf{s} + \mathbf{n} = \mathbf{d}. \tag{1}$$

Usually, signal $\mathbf{s}$ represents reflection events or geologic events, and noise $\mathbf{n}$ can be regarded as random noise or ground-roll noise. Let operators $\mathbf{S}$ and $\mathbf{N}$ denote the patterns of signal and noise, respectively. PEF is reasonable to be the pattern operator as it approximates the inverse energy spectrum of the corresponding component. Claerbout (2010) described the pattern operator as the absorbing operator, for instance, operator $\mathbf{N}$ may absorb noise $\mathbf{n}$ ($\mathbf{0} \approx \mathbf{Nn}$). And it can destroy the corresponding noise component from data $\mathbf{d}$ and leave signal $\mathbf{s}$:

$$\begin{aligned} \mathbf{0} &= \mathbf{N}(\mathbf{s} + \mathbf{n} - \mathbf{d}) \\ &= \mathbf{N}(\mathbf{s} + \mathbf{n}) - \mathbf{Nd} \\ &\approx \mathbf{Ns} - \mathbf{Nd} \ . \end{aligned} \tag{2}$$

Meanwhile, operator $\mathbf{S}$ absorbs or destroys signal component $\mathbf{s}$:

$$\mathbf{0} \approx \mathbf{Ss} \ , \tag{3}$$

which is used to restrict the shape of signal $\mathbf{s}$. By using above relationships, the pattern-based method raises a constrained least-squares problem, and solving such a problem can separate signal $\mathbf{s}$ and noise $\mathbf{n}$ from data volume $\mathbf{d}$.

$$\min_{\mathbf{s}} \| \ \mathbf{Ns} - \mathbf{Nd} \ \|_2^2 + \epsilon^2 \ \| \ \mathbf{Ss} \ \|_2^2 \ , \tag{4}$$

where $\epsilon > 0$ is the scaling factor of regularization term, which balancing the energy between estimated signal $\bar{\mathbf{s}}$ and noise $\bar{\mathbf{n}}$.

In practice, field data d and the noise model are often available, but the clean signal is not. We here considered the noise model to be a dataset containing the properties of noise $\mathbf{n}$, and the noise model can be obtained as a roughly separated noise section. Therefore, data pattern $\mathbf{D}$ and noise pattern $\mathbf{N}$ are easily estimated from the field data and noise model, while it cannot directly obtain signal pattern $\mathbf{S}$. Normally, one makes a compromise by replacing $\mathbf{S}$ with $\mathbf{D}$: with $\mathbf{D}$:

$$\min_{\mathbf{s}} \| \ \mathbf{Ns} - \mathbf{Nd} \ \|_2^2 + \epsilon^2 \ \| \ \mathbf{Ds} \ \|_2^2 \ , \tag{5}$$

where $\mathbf{D}$ may be unsuitable for constraining the shape of signal $\mathbf{s}$, and finally lead to undesirable separation result. Assuming that noise $\mathbf{n}$ and signal $\mathbf{s}$ are uncorrelated, Spitz (1999) proposed an approximation $\mathbf{S} = \mathbf{N}^{-1}\mathbf{D}$, which is based on the relationship between the pattern operator and the energy spectrum of the corresponding

component, and the regularization term becomes $\|\mathbf{N}^{-1}\mathbf{Ds}\|_2^2$. Furthermore, one can multiply equation 5 by $\mathbf{N}$ to avoid the acquisition of $\mathbf{N}^{-1}$:

$$\min_{\mathbf{s}} \| \mathbf{N}(\mathbf{Ns} - \mathbf{Nd}) \|_2^2 + \epsilon^2 \| \mathbf{N}(\mathbf{Ds}/\mathbf{N}) \|_2^2 , \tag{6}$$

then the signal-noise separation problem turns into:

$$\min_{\mathbf{s}} \| \mathbf{NNs} - \mathbf{NNd} \|_2^2 + \epsilon^2 \| \mathbf{Ds} \|_2^2 . \tag{7}$$

Equation 7 avoids the requirement for pattern operator $\mathbf{S}$ of the clean signal, and minimizing the equation leads to the expression of the estimated signal:

$$\bar{\mathbf{s}} = \left( \frac{\mathbf{N}^T\mathbf{NN}^T\mathbf{N}}{\mathbf{N}^T\mathbf{NN}^T\mathbf{N} + \epsilon^2\mathbf{D}^T\mathbf{D}} \right) \mathbf{d} , \tag{8}$$

and the formal solution of the estimated noise is:

$$\bar{\mathbf{n}} = \left( \frac{\epsilon^2\mathbf{D}^T\mathbf{D}}{\mathbf{N}^T\mathbf{NN}^T\mathbf{N} + \epsilon^2\mathbf{D}^T\mathbf{D}} \right) \mathbf{d} . \tag{9}$$

The conjugate gradient algorithm is implemented to calculate the numerical solution of equations 8 and 9 (Appendix section). We will discuss the estimation of the nonstationary pattern operators in the next section.

## Estimation of nonstationary pattern operators

Seismic events appear to be stationary in a small time-space window, but their behaviors will change with time and space. The patching method assumes seismic events with constant slope within the time-space window, which is used to deal with nonstationarity, but it may fail when encountering steeply changing slope. We consider here APEF as the pattern operator for better characterizing the pattern of nonstationary seismic data. Similar to decreasing the patch size to a data sample, the APEF without patching windows can handle the spectrum variability of seismic data in the time-space domain.

To estimate the nonstationary pattern of a 2D seismic section $d(t, x)$, prediction coefficients An of the APEF can be obtained as:

$$\bar{\mathbf{A}}_n(t,x) = \arg\min_{A_n} \| \mathbf{d}(t,x) - \sum_{n=1}^{N} \mathbf{A}_n(t,x)\mathbf{d}_n(t,x) \|_2^2 + \lambda^2 \sum_{n=1}^{N} \| \mathbf{R}[\mathbf{A}_n(t,x)] \|_2^2 , \tag{10}$$

where $\mathbf{d}_n(t,x) = \mathbf{d}(t-i, x-j)$ represents the adjacent data around $\mathbf{d}(t,x)$. $i$ and $j$ are the index of time shift and spatial shift, respectively. $\lambda$ is the scaling parameter and $\mathbf{R}[\bullet]$ is the shaping regularization operator Fomel (2009).

To obtain the whitening output, one needs to design APEF **D** of data with the causal filter structure. For example, a five-sample (time) × three-sample (space) template is shown as:

$$\begin{array}{ccc} . & A_3(t,x) & A_8(t,x) \\ . & A_4(t,x) & A_9(t,x) \\ 1 & A_5(t,x) & A_{10}(t,x) \\ A_1(t,x) & A_6(t,x) & A_{11}(t,x) \\ A_2(t,x) & A_7(t,x) & A_{12}(t,x) \end{array} . \tag{11}$$

The structure of filter coefficients influences the prediction result, and it could be limited by the range of local slope and the variability of seismic events along the space and time axes. For steeply dipping events, it suggests a large prediction window in the time direction. Obviously, the pattern of random noise is different from that of ground-roll noise, and we calculated noise pattern **N** according to the following approaches:

(i) Random noise: it supposes that the energy of random noise is spatially uncorrelated, and its statistical property may slightly change with time. To characterize the model of random noise, noise pattern N can be set as the shape of a column. The following is an example of the noise pattern structure with 4 (time) × 1 (space) coefficients:

$$\begin{array}{c} 1 \\ A_1(t,x) \\ A_2(t,x) \\ A_3(t,x) \end{array} . \tag{12}$$

We can generate a noise model containing the characteristics of noise **n**, and calculate APEF **N** from the noise model. Also, one can directly estimate APEF **N** of random noise from dataset **d**, especially when there exists strong random noise in the dataset. **N** with one-column shape can only capture the temporal spectrum of random noise, but ignores the signal predictability along the space direction in the dataset.

(ii) Ground-roll noise: due to the difference of the dominant frequency, ground-roll noise and the effective signal can usually be separated in the frequency domain. Using a low-pass filter to the data can produce a noise model. Similarly, according to the difference of slowness, the primaries can be muted in the radon domain, and a ground-roll noise model can be obtained through the inverse radon transform. Here, we first use a reliable low-pass filter to generate the ground-roll noise model, then APEF **N** of the ground-roll noise is calculated according to the structure similar to that of data as equation 11. Due to the slower speed of the ground-roll noise, it has steep events with larger local slope, and the filter size needs to be adjusted to a larger length in the time direction.

Therefore, the proposed signal-noise separation method exploits a two-step strategy: (i) estimating data pattern **D** and noise pattern **N** by using the APEF, and (ii) separating signal and noise with the pattern-based method (equation 7). The further

examination of the proposed method will be shown in the data examples section.

# DATA EXAMPLES

## Nonstationary signal and random noise separation

We started with a synthetic model (figure 1a) containing a curve event with varying slope. Figure 1b is the model data with the white Gaussian noise added. The F-K spectra (figure 2) show that the strong random noise severely affects the curve model. For comparison, we first used FXDECON, a standard industry method, to separate the signal from the noisy data. We designed the FXDECON with four-sample (space) filter size and ten-sample (space) sliding window. Although the FXDECON method results in a highest SNR (Table 1), it still fails to deal with strong random noise. The strong random noise has been suppressed in the estimated signal section (figure 3a), but a large part of signal is also destroyed and leaves the estimated noise section (figure 3b). Due to the strong energy of the random noise, the high SNR is caused by the suppression of both noise and signal. To demonstrate the effectiveness of the proposed nonstationary APEF, we separated the random noise using the pattern-based method (equation 7) with the stationary PEF in the t-x domain. The filter size of data pattern (PEF) D is selected with 11 (time) $\times$ 4 (space), noise pattern (PEF) N is 5 (time) $\times$ 1 (space) coefficients. Figure 3c shows that the stationary approach fails in separating the random noise in the estimated signal section as the stationary PEF is hard to characterize the nonstationary data pattern. Meanwhile, some energy appears from the signal in the estimated noise section (figure 3d). Figure 3e shows the denoised result of the curvelet transform with percentage threshold; this method effectively suppresses the random noise in the range from about 30 to 100 Hz (figure 4c), but it generates striped noise interference that affects the quality of the synthetic model. For the proposed method, we configured the APEF with the same filter size as that of the stationary PEF. The smoothing radii in the time and space directions for data pattern (APEF) $\mathbf{D}$ is selected to be 30 and 15 samples, respectively. And the noise pattern (APEF) $\mathbf{N}$ has a 300-sample (time) $\times$ 1-sample (space) smoothing radius. Figure 3g contains a part of the low-level noise, while the curve event has been recovered. The proposed method shows better signal protection ability, and obtains the denoised result at a high SNR level (Table 1). Here the SNR is calculated by equation 13:

$$SNR = 10\log_{10}\left(\frac{\|\mathbf{s}\|_2^2}{\|\mathbf{s}-\bar{\mathbf{s}}\|_2^2}\right) \tag{13}$$

where $\mathbf{s}$ denotes effective signal, $\bar{\mathbf{s}}$ denotes denoised result. In the F-K spectra (figure 4), the energy of the curve event can be identified only in the denoised results using the curvelet transform and proposed method.

Figure 5 shows a poststack section, where the random noise influences the continuity of the reflection events. The data includes dipping beds and a fault. The main challenge in this example is that the random noise displays the nonstationary

| | Synthetic model | FXDECON | Stationary PEF | Curvelet transform | The proposed method |
|---|---|---|---|---|---|
| SNR | -9.432 | -3.957 | -5.176 | -5.414 | -5.029 |

Table 1: Comparison of the SNR of the random noise attenuation results

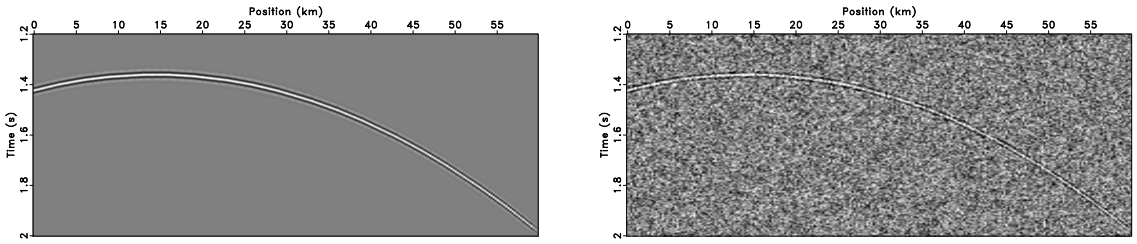


(a) (b)

Figure 1: (a) Clean data with curve event and (b) data with random noise.

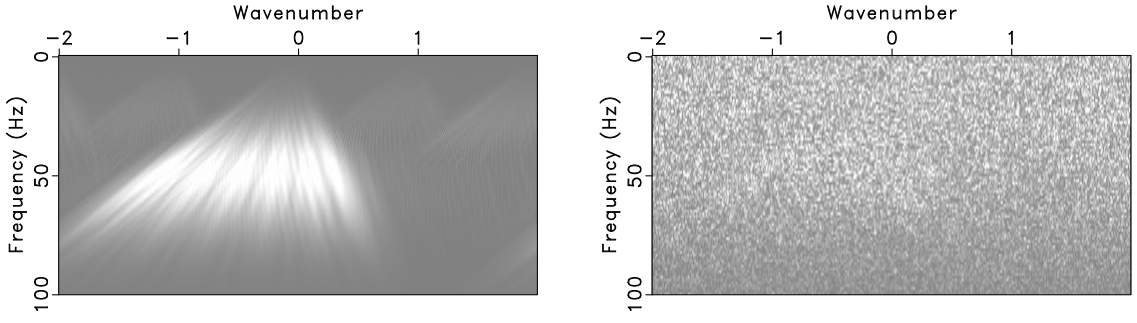


(a) (b)

Figure 2: (a) F-K spectra of clean data and (b) noisy data.

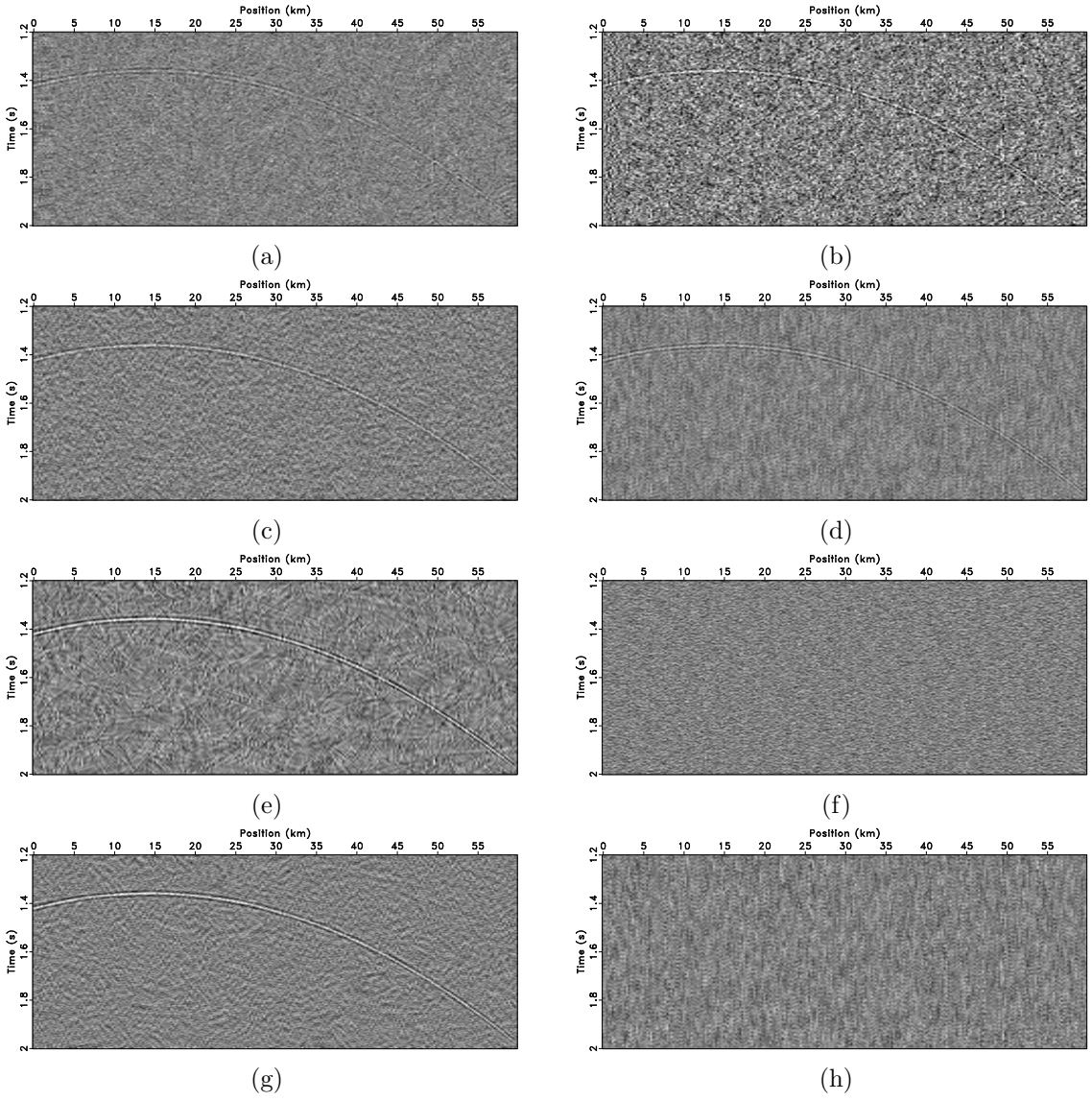


Figure 3: (a) Estimated signal and (b) random noise by the FXDECON. (c) Estimated signal and (d) random noise by the pattern-based method with the stationary PEF. (e) Estimated signal and (f) random noise by the curvelet transform. (g) Estimated signal and (h) random noise by the proposed method.

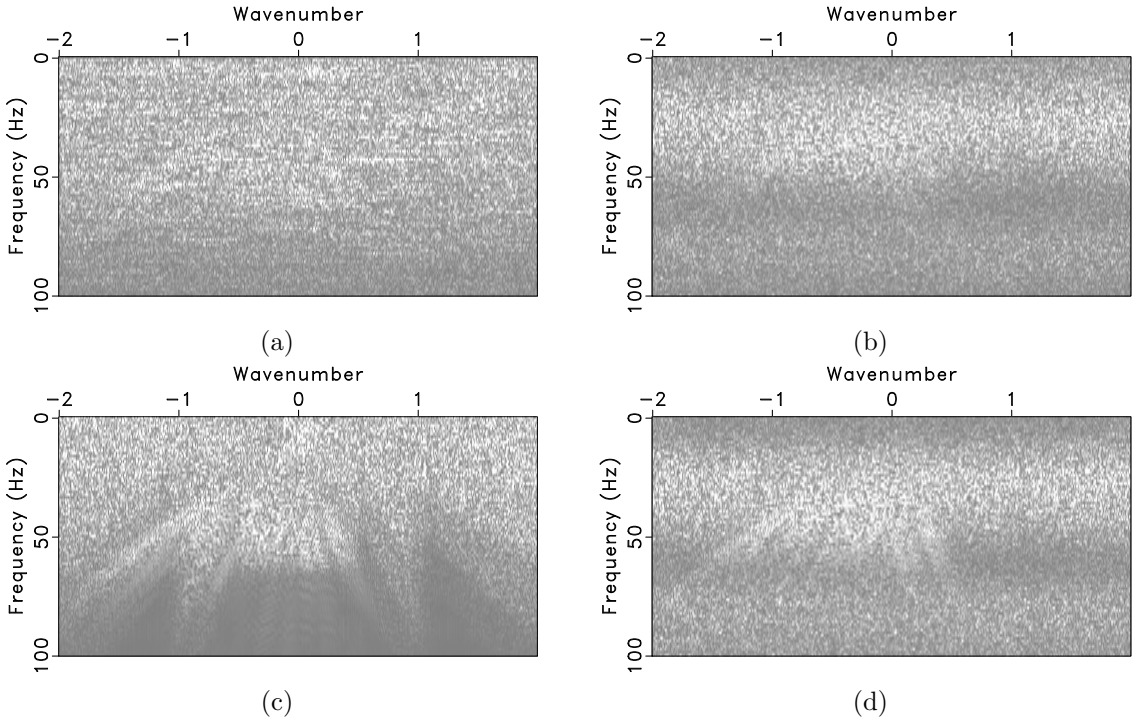


Figure 4: (a)F-K spectrum of the denoised result using the FXDECON. (b) F-K spectrum of the denoised result using the pattern-based method with the stationary PEF. (c) F-K spectrum of the denoised result using the curvelet transform. (d) F-K spectrum of the denoised result using the proposed method.

energy distribution. Figure 6 shows the separation results by using FXDECON, the filter size has eight sample (space) coefficients for each data sample and a 30-sample (space) sliding window for handling the variation of the signals. The FXDECON method fails in separating the nonstationary signal and random noise; weak energy random noise is still present in the signal section (figure 6a) and part of the signal leaks into the noise section (figure 6b). By using the pattern-based method with the stationary PEF, we got the denoised result in figure 7. The data pattern (PEF) **D** is selected with 11 (time) $\times$ 4 sample (space) coefficients, noise pattern (PEF) **D** has 9 (time) $\times$ 1 sample (space) coefficients. In figure 7, the denoised result contains some high frequency noise, and part of the signal is removed. As shown in figure 10b, the energy of effective signal at about 18 Hz is partially filtered out. In the denoised result of curvelet transform with percentage threshold (figure 8), the random noise causes a stronger smearing of the events. Then we deal with the post- stack section by using the proposed method. The data APEF **D** has 9 (time) $\times$ 4 sample (space) coefficients for each sample and the smoothing radius is selected to be 60 (time) and 20 samples (space). The noise APEF **N** is designed as a 9 (time) $\times$ 1 sample (space) coefficients with a 60 (time) $\times$ 1 sample (space) smoothing radius. The estimated signal section displays that the continuity of the reflection layers with better smoothness is enhanced, and the fault is well preserved (figure 9a). The energy of the events and fault hardly leak into the noise section (figure 9b). The F-K spectrum in figure 10d is cleaner and the effective signal energy is concentrated. It indicates that the proposed method has a better capability for noise suppression and signal protection than other methods.

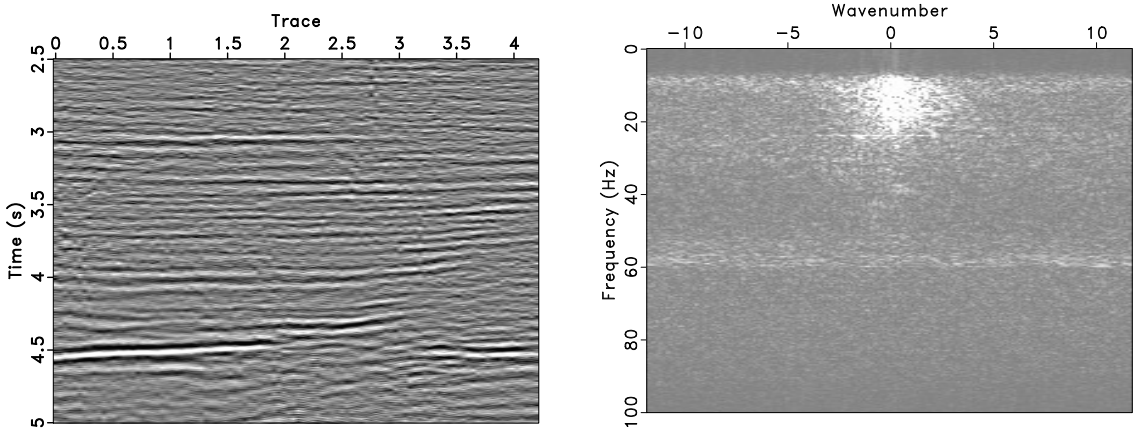


(a) (b)

Figure 5: (a) Poststack section with random noise and (b) the corresponding F-K spectrum.

## Nonstationary signal and ground-roll noise separation

As a kind of coherent noise in land survey, ground-roll noise always displays high amplitude, low frequency and low velocity. We created a synthetic model to examine

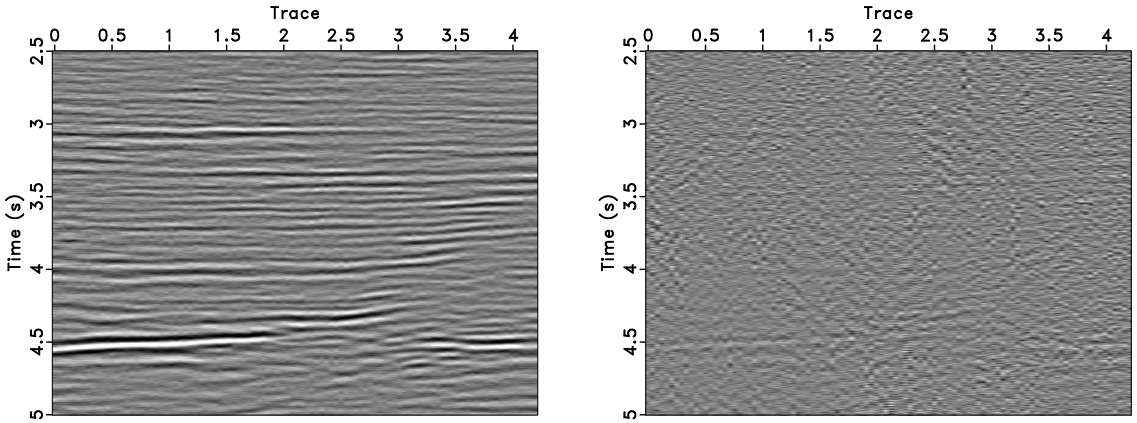


(a) (b)

Figure 6: Random noise separation results of the poststack section using the FXDECON. (a) Section of estimated signal and (b) section of separated random noise.

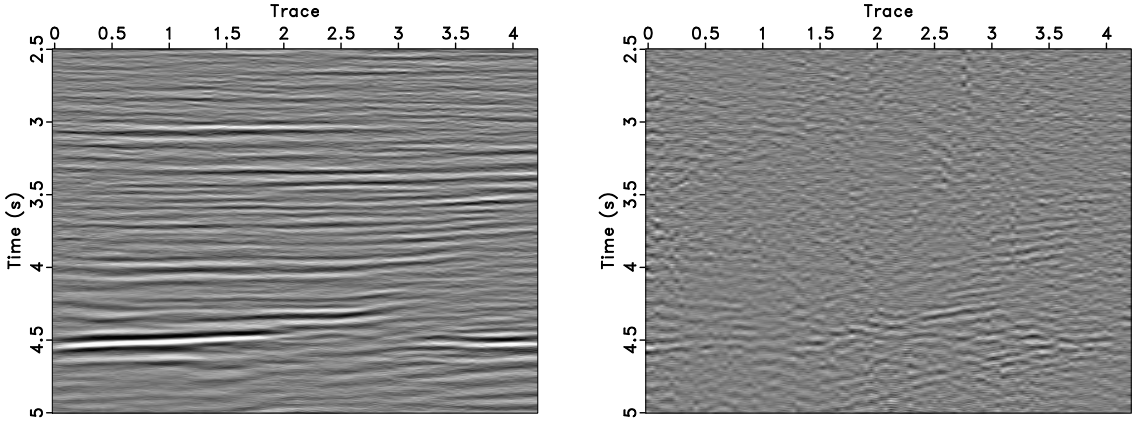


(a) (b)

Figure 7: Random noise separation results of the poststack section using the pattern-based method with the stationary PEF. (a) Section of estimated signal and (b) section of separated random noise.

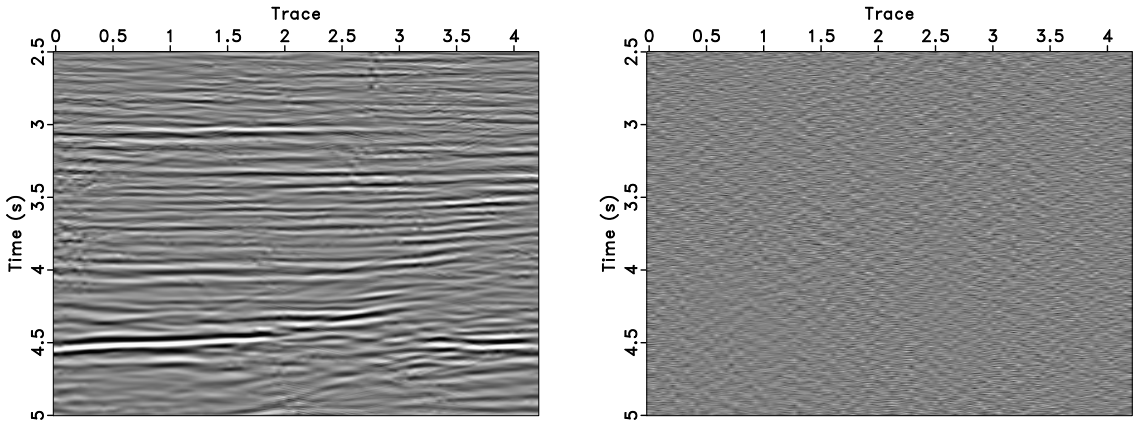


(a) (b)

Figure 8: Random noise separation results of the poststack section using the curvelet transform. (a) Section of estimated signal and (b) section of separated random noise.

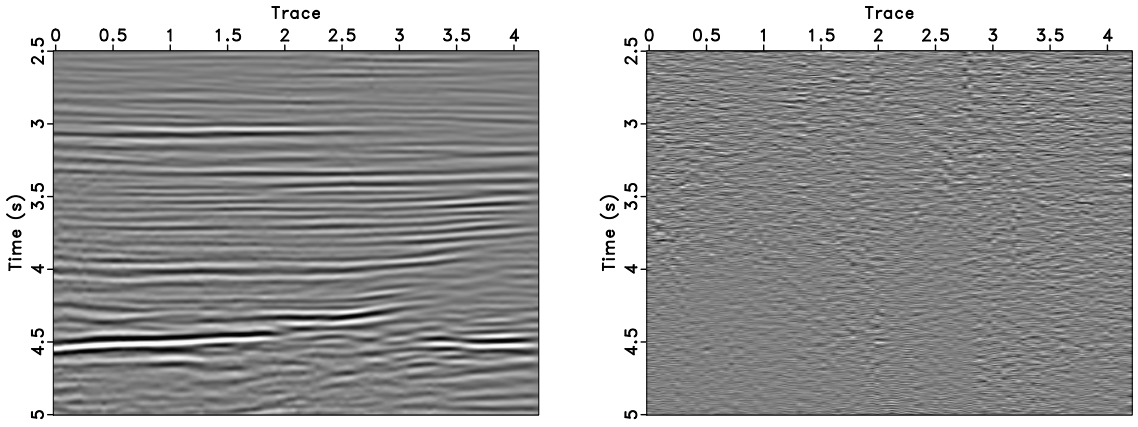


(a) (b)

Figure 9: Random noise separation results of the poststack section using the proposed method. (a) Section of estimated signal and (b) section of separated random noise.

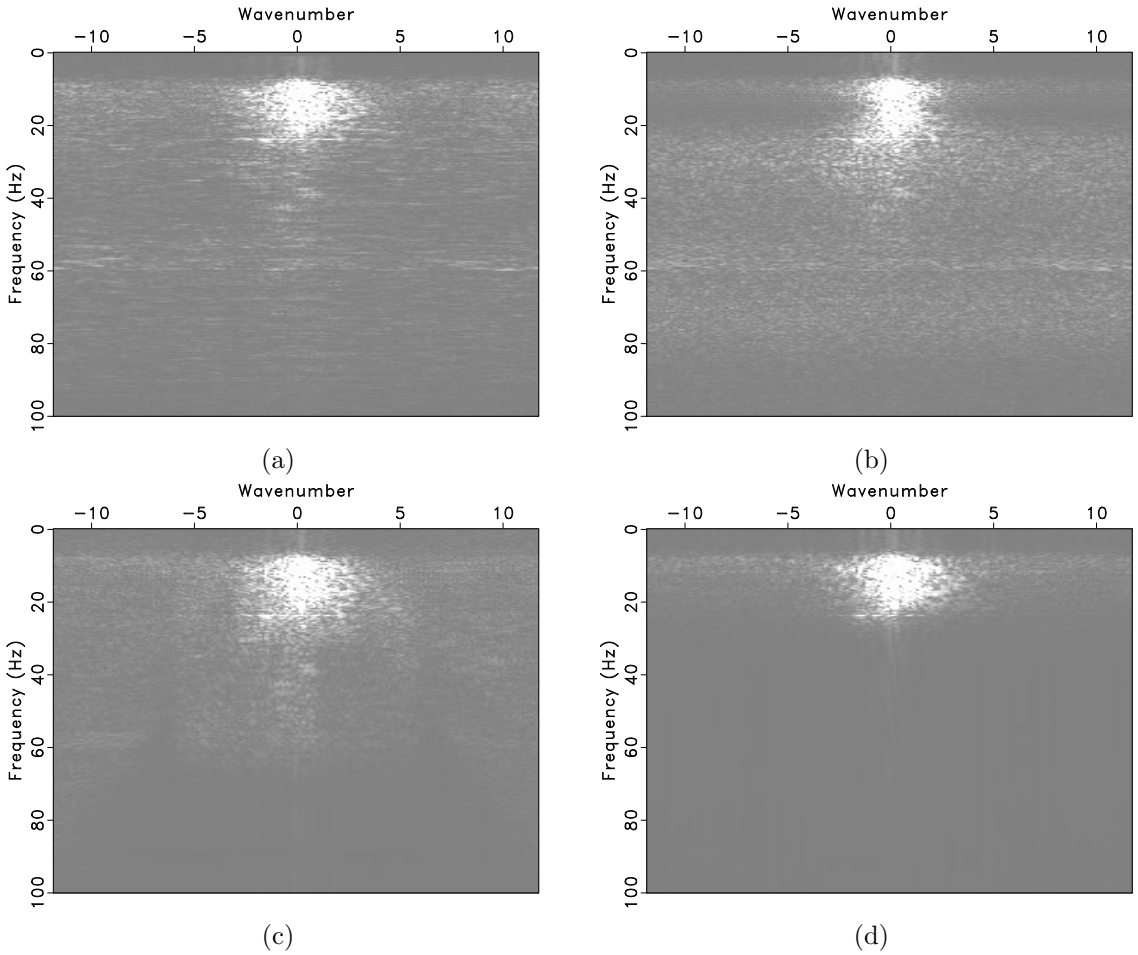


Figure 10: (a)F-K spectrum of the denoised result using the FXDECON. (b) F-K spectrum of the denoised result using the pattern-based method with the stationary PEF. (c) F-K spectrum of the denoised result using the curvelet transform. (d) F-K spectrum of the denoised result using the proposed method.

the validity of the proposed method (figure 11a). The shot gather has low-frequency ground-roll noise and four hyperbolic reflection events, which overlap in the frequency domain (figure 11b). The linear ground-roll noise is generated by combining linear events with different dominant frequency, and its frequency range is limited from 0 to about 30 Hz. For comparison, the high-pass filter with a 25-Hz cutoff frequency produces the ground-roll noise separation result (figure 12). The nonstationary signal and ground-roll noise show the energy leakage in each other's sections because the frequency bandwidth of the ground-roll noise overlaps with that of the reflection events. Figure 13 shows the noise separation result by using the local time-frequency (LTF) decomposition (Liu and Fomel, 2013). In the time-frequency-space domain, we designed a muting filter to remove the ground-roll noise components, which leads to a higher SNR result (Table 2). By using the proposed method, the ground-roll noise can be separated in to the following steps (Fomel, 2002):

(i) Use a low-pass filter to roughly separate the ground-roll noise as an initial estimation.
(ii) Make a mask from the initial noise model, and subsequent separation process is restricted in this time-space window.
(iii) Calculate noise pattern $\mathbf{N}$ from the noise model using APEF.
(iv) Calculate data pattern $\mathbf{D}$ from the origin data using APEF.
(v) Further separate the signal and ground-roll noise based on equation 7.

The noise model is made by the low-pass filter with a 12-Hz cutoff frequency. We selected 12 (time) $\times$ 3 samples (space) filter coefficients for noise APEF $\mathbf{N}$ to predict the energy of the steep ground-roll noise, the smoothing radius is set to be 20 (time) $\times$ 10 samples (space). Meanwhile, data APEF $\mathbf{D}$ has 7 (time) $\times$ 4 samples (space) filter coefficients, the smoothing radius is 40 (time) $\times$ 30 samples (space). The separated signal by using the proposed method is well recovered (figure 14a), and the SNR of the denoised results is comparable to that of LTF decomposition (Table 2). The estimated noise section further verifies the successful signal-noise separation (figure 14b). Although some noise at low frequency is still present (figure 15d) and affects the SNR, the energy of the effective signal is much cleaner after using the proposed method.

| | Synthetic model | High-pass filtering | LTF decomposition | The proposed method |
|---|---|---|---|---|
| SNR | -13.3 | 6.514 | 8.988 | 8.001 |

Table 2: Comparison of the SNR of the ground-roll noise separation results

Figure 16 shows the profile and the corresponding spectrum of a 3D land shot gather from Saudi Arabia, where the ground-roll noise is three-dimensional and appears as a hyperbolic shape in this receiver line. Due to the difference of dominant frequency between the ground-roll noise and reflection events, it may suggest separating them based on different frequency. The frequency-based separation method

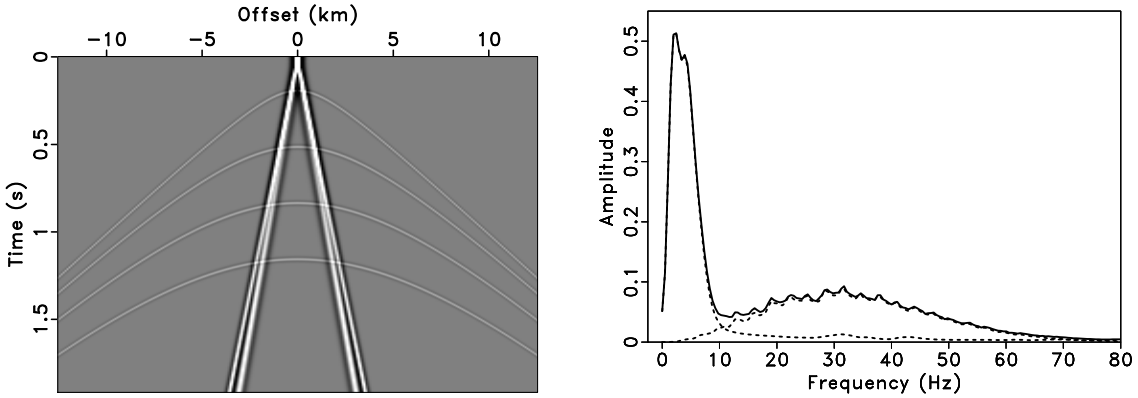


(a) (b)

Figure 11: (a) Synthetic shot gather containing ground-roll and (b) comparison of the spectrum. Solid line is the synthetic model, dashed lines the ground-roll noise (5 Hz dominant frequency) and reflection events (30 Hz dominant frequency).

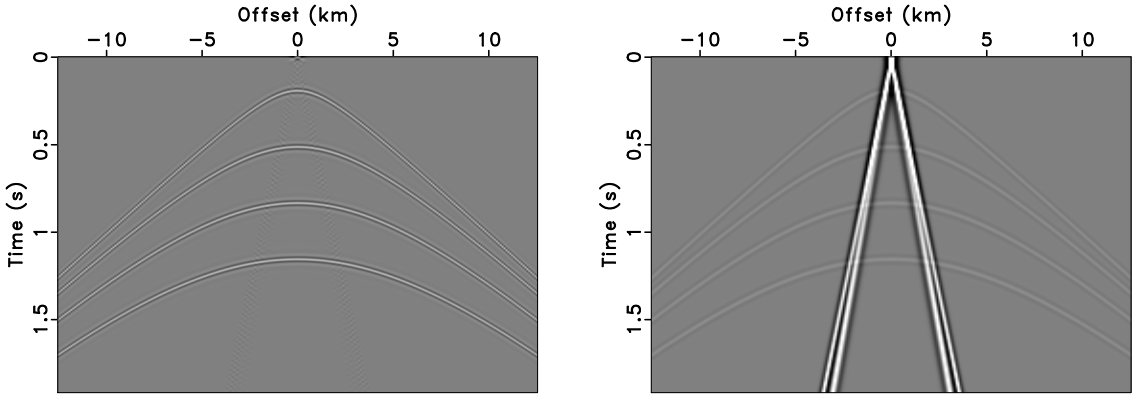


(a) (b)

Figure 12: Noise separation results of the synthetic shot gather using the high-pass filtering. (a) Section of estimated signal and (b) section of separated ground-roll noise.

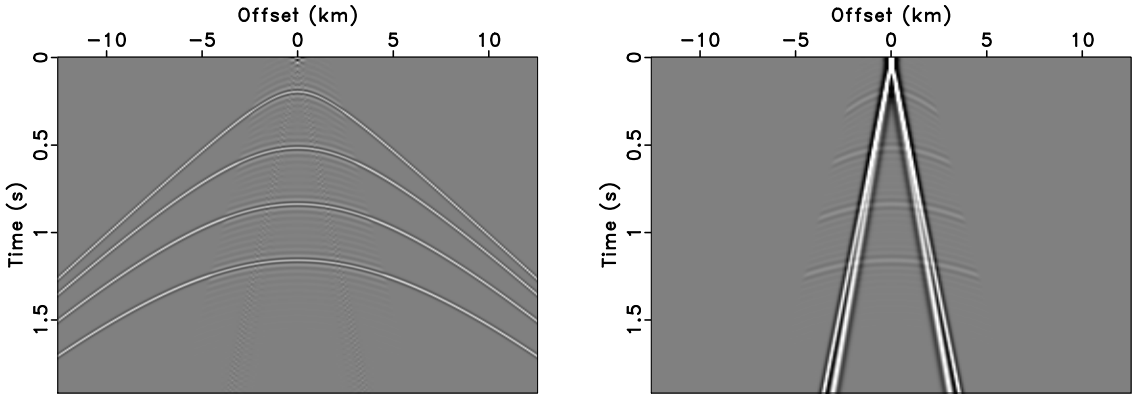


(a) (b)

Figure 13: Noise separation results of the synthetic shot gather using the LTF decomposition. (a) Section of estimated signal and (b) section of separated ground-roll noise.

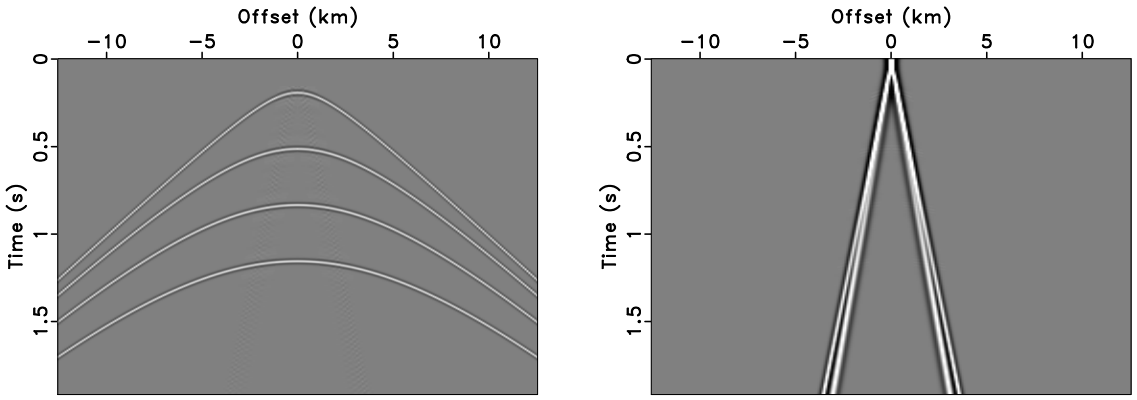


(a) (b)

Figure 14: Noise separation results of the synthetic shot gather using the proposed method. (a) Section of estimated signal and (b) section of separated ground-roll noise.

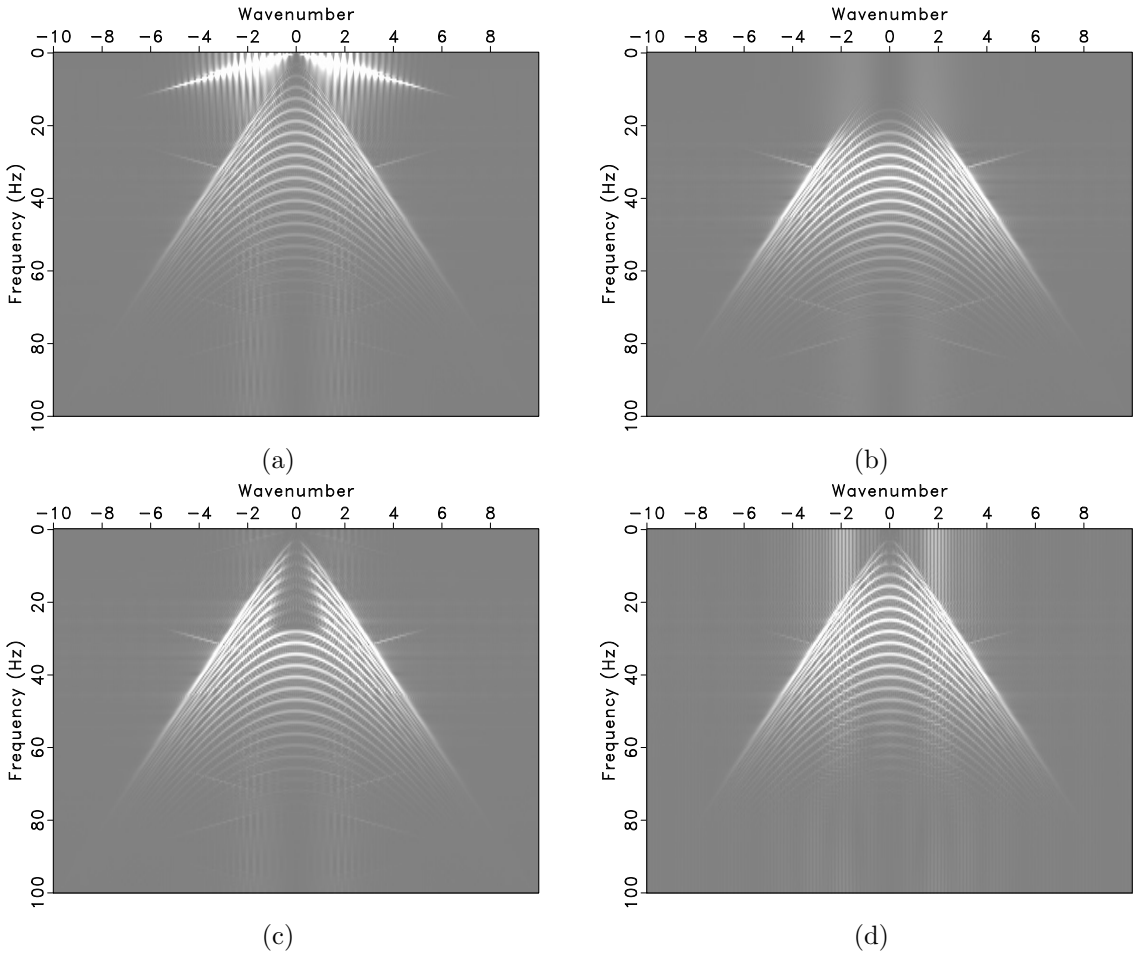


Figure 15: (a) F-K spectrum of the synthetic model. (b) F-K spectrum of the denoised result using the high-pass filtering. (c) F-K spectrum of the denoised result using the LTF decomposition. (d) F-K spectrum of the denoised result using the proposed method.

leads to a worse result with a simple filter design, and the estimated signal by using the high-pass filter with 20-Hz cutoff frequency contains more low-level ground-roll noise (figure 17a). The LTF decomposition method with a carefully selected muting filter gets better results than those from high-pass filtering, but it still leaves some ground-roll noise in the middle part of the estimated signal section (figure 18a). We used the initial noise model (figure 17b) to characterize the ground-roll noise, noise APEF $\mathbf{N}$ is designed with 12 (time) $\times$ 3 samples (space) filter size and 20 (time) $\times$ 15 samples (space) smoothing radius. Data APEF $\mathbf{D}$ uses a smaller filter size with 5 (time) $\times$ 4 samples (space) coefficients and 30 (time) $\times$ 25 samples (space) smooth radius to capture signal energy. In the F-K spectrum (figure 20d), there are also some weaker energies below 20 Hz, but the ground-roll noise has been separated from the denoised results (figure 19a). The proposed method achieved the separation goal that the underlying reflection events clearly appear in the estimated section, and the ground-roll noise is well suppressed.

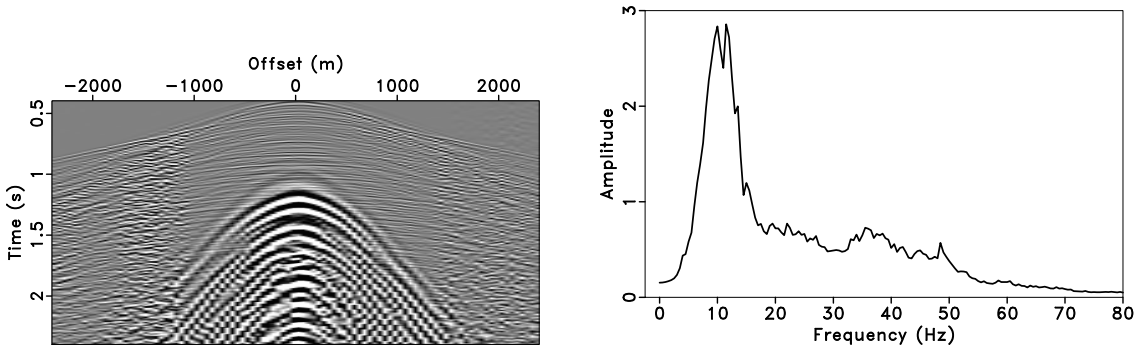


(a) (b)

Figure 16: (a) A receiver line of the 3D shot gather and (b) the corresponding spectrum.

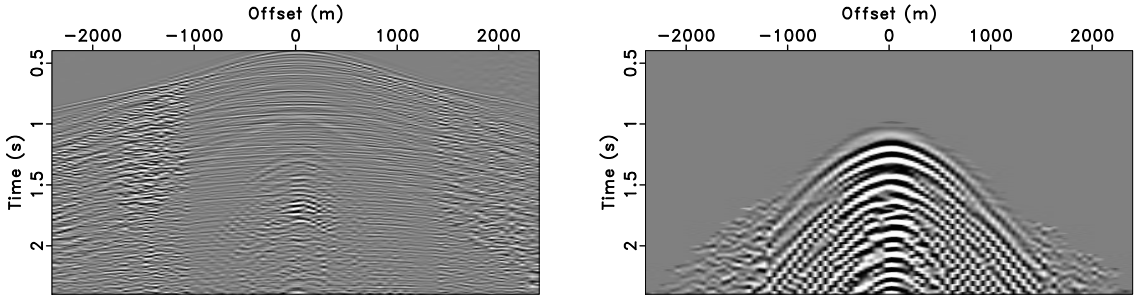


(a) (b)

Figure 17: Noise separation results of the field data using the high-pass filtering. (a) Section of estimated signal and (b) section of separated ground-roll noise.

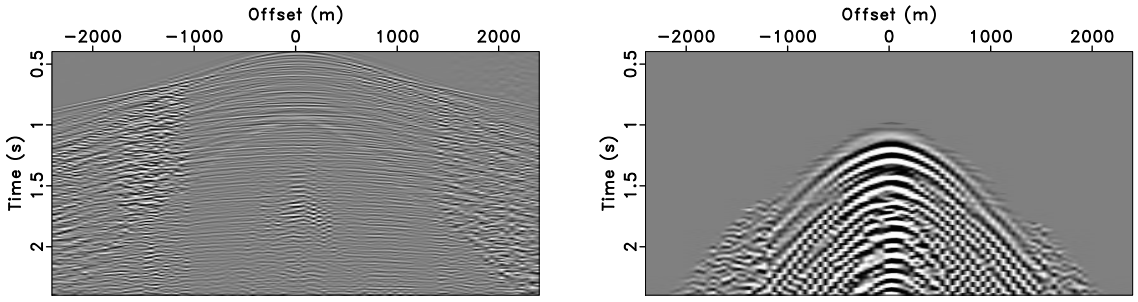


(a) (b)

Figure 18: Noise separation results of the field data using the LTF decomposition. (a) Section of estimated signal and (b) section of separated ground-roll noise.

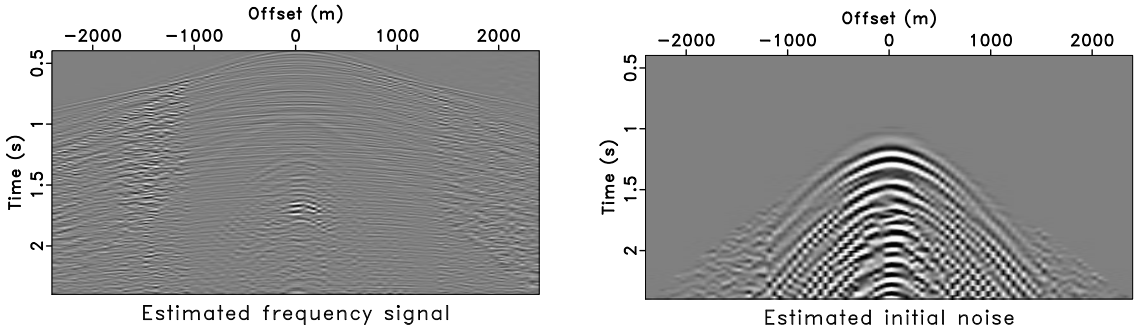


(a) (b)

Figure 19: Noise separation results of the field data using the proposed method. (a) Section of estimated signal and (b) section of separated ground-roll noise.

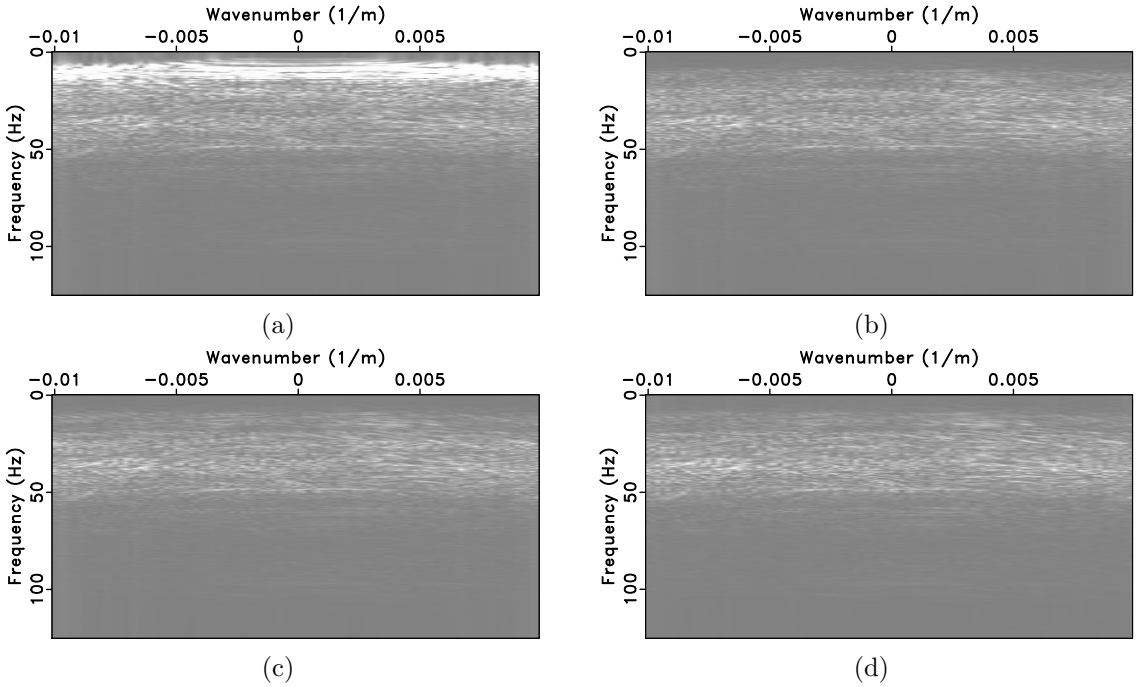


Figure 20: (a) F-K spectrum of the shot gather. (b) F-K spectrum of the denoised result using the high-pass filtering. (c) F-K spectrum of the denoised result using the LTF decomposition. (d) F-K spectrum of the denoised result using the proposed method.

## DISCUSSION

We considered that the APEF can characterize the properties of data and treated the corresponding APEF as the pattern operator. Data pattern operator $\mathbf{D}$ and noise pattern operator $\mathbf{N}$ can be obtained by solving the corresponding APEF. Since APEF uses the shaping regularization constraint, there are two main parameters that affect the filter: one is the filter size, and the other is the smoothing radius (Liu et al., 2011). These two parameters are empirical, and they are related to the characteristics of the events, including spatial distribution, local slope, etc. We applied the pattern operators to the corresponding dataset and adjusted the parameters of the APEF by observing whether the corresponding data components were absorbed or not. For example, the noise component can be absorbed by using pattern operator $\mathbf{N}$ in the noise model ($\mathbf{0} \approx \mathbf{Nn}$).

## CONCLUSION

We introduced a new pattern-based approach for nonstationary signal-noise separation. Our method used the APEF as the pattern operator, which was suitable for characterizing the nonstationary properties of seismic data and noise in the time-space domain. After calculating the data pattern $\mathbf{D}$ and the noise pattern $\mathbf{N}$, we could separate the signal and noise by solving a constrained least-squares problem. We adopted different algorithms to deal with the random noise and ground-roll noise separation problem. Numerical examples showed that the proposed method provided a robust signal-noise separation, even in the presence of random noise with nonstationary energy distribution and strongly curved ground roll. Multiple suppression and diffraction separation were also other applications of this method.

## ACKNOWLEDGEMENT

Thanks to Sergey Fomel for the enlightening discussion. This work is supported by the National Natural Science Foundation of China (grant nos. 41974134, 41874125, and 41774127) and the National key Research and Development Program of China (grant no. 2018YFC0603701).

## CONJUGATE GRADIENT ALGORITHM

The pattern-based method can be described as the constrained linear equation system:

$$\mathbf{0} \approx \mathbf{NNs} - \mathbf{NNd0} \quad \approx \epsilon \mathbf{Ds} \tag{A-1}$$

where $\mathbf{NN}$ denotes the chain operator, which applies operator $\mathbf{N}$ twice. The following conjugate gradient algorithm (Wang, 2016) can be used to solve such problem.
CONJUGATE GRADIENTS WITH REGULARIZATION($\mathbf{NN}, \mathbf{S}, \mathbf{d}, \mathbf{s}, \epsilon$)

$\mathbf{s} \leftarrow \mathbf{0}$
$\mathbf{r} \leftarrow -\mathbf{NNd}$
**for** $n \leftarrow 1, 2, \ldots, Niter$
  **do**
    $\mathbf{g} \leftarrow \mathbf{N}\mathbf{N}^T\,\mathbf{r} + \epsilon\,\mathbf{S}^T\,\mathbf{s}$
    $\mathbf{G} \leftarrow \mathbf{NN}\,\mathbf{g} + \epsilon\,\mathbf{S}\,\mathbf{g}$
    $\rho \leftarrow \mathbf{g}^T\,\mathbf{g}$
    **if** $n = 1$
      **then** $\beta \leftarrow 0$
      **else** $\beta \leftarrow \rho/\hat{\rho}$
    $\begin{bmatrix} \mathbf{p} \\ \mathbf{P} \end{bmatrix} \leftarrow \begin{bmatrix} \mathbf{g} \\ \mathbf{G} \end{bmatrix} + \beta \begin{bmatrix} \mathbf{p} \\ \mathbf{P} \end{bmatrix}$
    $\alpha \leftarrow -\rho/(\mathbf{P}^T\,\mathbf{P})$
    $\begin{bmatrix} \mathbf{s} \\ \mathbf{r} \end{bmatrix} \leftarrow \begin{bmatrix} \mathbf{s} \\ \mathbf{r} \end{bmatrix} + \alpha \begin{bmatrix} \mathbf{p} \\ \mathbf{P} \end{bmatrix}$
    $\hat{\rho} \leftarrow \rho$
**return s**

## REFERENCES

Bednar, J. B., and G. H. Neale, 1999, A comparison of pattern and series based multiple suppression: 69th Annual International Meeting, SEG, Expanded Abstracts, 1056–1059.

Brown, M., and R. G. Clapp, 2000, (t,x) domain, patern-based ground roll removal: 70th Annual International Meeting, SEG, Expanded Abstracts, 2103–2106.

Canales, L. L., 1984, Random noise reduction: 54th Annual International Meeting, SEG, Expanded Abstracts, 525–527.

Claerbout, J. F., 2010, Image estimation by example: Geophysical soundings image construction - Multidimensional autoregression: Stanford Exploration Project, http://sepwww.stanford.edu/sep/prof/.

Claerbout, J. F., and S. Fomel, 2000, Spitz makes a better assumption for the signal PEF: SEP report, **103**, 205–213.

Claerbout, J. F., and A. G. Johnson, 1971, Extrapolation of Time-Dependent Waveforms along their Path of Propagation: Geophysical Journal International, **26**, 285–293.

Corso, G., P. S. Kuhn, L. S. Lucena, and Z. D. Thom, 2003, Seismic ground roll timefrequency filtering using the gaussian wavelet transform: Physica A: Statistical Mechanics and its Applications, **318**, 551–561.

Fomel, S., 2002, Applications of plane-wave destruction filters: Geophysics, **67**, 1946–1960.

———, 2009, Adaptive multiple subtraction using regularized nonstationary regression: Geophysics, **74**, V25–V33.

Fomel, S., and Y. Liu, 2010, Seislet transform and seislet frame: Geophysics, **75**, V25–V38.

Guitton, A., 2006, A patternbased approach for multiple removal applied to a 3d gulf of mexico data set: Geophysical prospecting, **54**, 135–152.

Kumar, V., and F. J. Herrmann, 2009, Incoherent noise suppression with curvelet-domain sparsity: 79th Annual International Meeting, SEG, Expanded Abstracts, 3356–3360.

Liu, G., X. Chen, and K. Wu, 2011, Random noise attenuation using nonstationary autoregression in F-X domain: 73rd Annual International Meeting, EAGE, Expanded Abstracts, P091.

Liu, Y., and S. Fomel, 2013, Seismic data analysis using local time-frequency decomposition: Geophysical Prospecting, **61**, 516–525.

Liu, Y., S. Fomel, and C. Liu, 2015, Signal and noise separation in prestack seismic data using velocity-dependent seislet transform: Geophysics, **80**, WD117–WD128.

Liu, Y., and B. Li, 2018, Streaming orthogonal prediction filter in the t-x domain for random noise attenuation: Geophysics, **83**, F41–F48.

Miao, X., and S. Cheadle, 1998, Noise attenuation with wavelet transforms: 68th Annual International Meeting, SEG, Expanded Abstracts, 1072–1075.

Naghizadeh, M., and M. Sacchi, 2018, Ground-roll attenuation using curvelet downscaling: Geophysics, **83**, V185–V195.

Spitz, S., 1999, Pattern recognition, spatial predictability, and subtraction of multiple events: The Leading Edge, **18**, 55–58.

Trad, D. O., T. J. Ulrych, and M. D. Sachhi, 2002, Accurate interpolation with highresolution timevariant radon transforms: Geophysics, **67**, 644–656.

Wang, Y., 1999, Random noise attenuation using forward-backward linear prediction: Journal of Seismic Exploration, **8**, 133–142.

———, 2016, Seismic Inversion: Theory and Applications: Wiley Blackwell.

Yu, S., J. Ma, and W. Wang, 2019, Deep learning for denoising: Geophysics, **84**, V333–V350.

Yuan, Y., X. Si, and Y. Zheng, 2020, Ground-roll attenuation using generative adversarial networks: Geophysics, **85**, WA255–WA267.